SLEEPJ, 2019, 1–13

doi: 10.1093/sleep/zsy230
Advance Access Publication Date: 21 November 2018
Original Article

ORIGINAL ARTICLE

Intra-"cortical" activity during avian non-REM and REM sleep: variant and invariant traits between birds and mammals

Jacqueline van der Meij[1], Dolores Martinez-Gonzalez[1], Gabriël J. L. Beckers[2,†,*] and Niels C. Rattenborg[1,†,*]

[1]Avian Sleep Group, Max Planck Institute for Ornithology, Eberhard-Gwinner-Strasse 5, Seewiesen, Germany and [2]Cognitive Neurobiology and Helmholtz Institute, Utrecht University, Yalelaan 2, CM Utrecht, The Netherlands

Work Performed: Max Planck Institute for Ornithology, Seewiesen, Germany

*Corresponding authors. Niels Rattenborg, Avian Sleep Group, Max Planck Institute for Ornithology, Eberhard-Gwinner-Strasse 5, 82319 Seewiesen, Germany. Email: rattenborg@orn.mpg.de; Gabriël Beckers, Cognitive Neurobiology and Helmholtz Institute, Utrecht University, Yalelaan 2, 3584 CM Utrecht, The Netherlands. Email: g.j.l.beckers@uu.nl.

†These authors contributed equally to this work.

Abstract

Several mammalian-based theories propose that the varying patterns of neuronal activity occurring in wakefulness and sleep reflect different modes of information processing. Neocortical slow-waves, hippocampal sharp-wave ripples, and thalamocortical spindles occurring during mammalian non-rapid eye-movement (NREM) sleep are proposed to play a role in systems-level memory consolidation. Birds show similar NREM and REM (rapid eye-movement) sleep stages to mammals; however, it is unclear whether all neurophysiological rhythms implicated in mammalian memory consolidation are also present. Moreover, it is unknown whether the propagation of slow-waves described in the mammalian neocortex occurs in the avian "cortex" during natural NREM sleep. We used a 32-channel silicon probe connected to a transmitter to make intracerebral recordings of the visual hyperpallium and thalamus in naturally sleeping pigeons (*Columba livia*). As in the mammalian neocortex, slow-waves during NREM sleep propagated through the hyperpallium. Propagation primarily occurred in the thalamic input layers of the hyperpallium, regions that also showed the greatest slow-wave activity (SWA). Spindles were not detected in both the visual hyperpallium, including regions receiving thalamic input, and thalamus, using a recording method that readily detects spindles in mammals. Interestingly, during REM sleep fast gamma bursts in the hyperpallium (when present) were restricted to the thalamic input layers. In addition, unlike mice, the decrease in SWA from NREM to REM sleep was the greatest in these layers. Taken together, these variant and invariant neurophysiological aspects of avian and mammalian sleep suggest that there may be associated mechanistic and functional similarities and differences between avian and mammalian sleep.

Statement of Significance

Intra-cortical recordings have systematically characterized the neurophysiology of non-rapid eye-movement (NREM) and rapid eye-movement (REM) sleep in mammals, but not birds. In our intra-"cortical" recordings of the primary visual "cortex" (hyperpallium) of pigeons during NREM sleep, slow-waves usually appear first in thalamic input layers, as in mammals, and propagate within these layers, suggesting a common role for thalamic input in the genesis of slow-waves. Nonetheless, thalamocortical spindles were not detected in the hyperpallium or thalamus. Moreover, REM sleep–related changes in thalamic input layer slow-waves differed from the primary visual cortex of mice. The similarities and differences in thalamocortical network activity between mammals and birds during NREM and REM sleep could inform our understanding of the mechanisms and functions of mammalian sleep-related brain activity.

Key words: avian; NREM sleep; slow-waves; propagation; spindles; REM sleep; cortex

Submitted: 10 August, 2018; **Revised:** 10 October, 2018

Introduction

Shifting from wakefulness to sleep is marked by distinct changes in neuronal activity in the mammalian neocortex. During non-rapid eye-movement (NREM) sleep, the slow (<1 Hz) alternation in neuronal membrane potentials between hyperpolarized down-states with neuronal quiescence and depolarized up-states with action potentials gives rise to slow-waves in local field potential (LFP) and electroencephalogram (EEG) recordings [1], which propagate horizontally across the neocortex [2–4]. Interestingly, although REM sleep is traditionally characterized by EEG activation, intra-cortical recordings of mice recently revealed that slow-waves also occur in layer 4 of the primary sensory cortices during REM sleep [5].

The functions of slow-waves and their propagation remain unresolved [6]. Slow-waves occurring during NREM sleep have been implicated in various forms of synaptic scaling [7, 8]. Slow-waves occurring in conjunction with thalamocortical spindles and hippocampal sharp-wave ripples (SWRs) are also thought to be involved in the systems-level processing of hippocampal-dependent memories in mammals [9–13]. The propagation of slow-waves, per se, may be involved in processing information across neocortical areas via spike-timing-dependent plasticity [2, 6, 14, 15]. Finally, it has been proposed that slow-waves occurring in the thalamic input layer of primary sensory cortices of mice during REM sleep gate sensory input to the neocortex during this otherwise activated brain state [5].

Determining how neuronal activity flows through the neocortex during NREM sleep is essential for understanding sleep's role in processing information. Both the neocortex and thalamus have been implicated in the genesis of slow-waves occurring during NREM sleep [16–18]. In naturally sleeping cats, up-states appear first within layer 5 [19], a layer that along with layer 4 receives thalamic input [20], and then propagate vertically within a column to layer 4 and the supragranular layers [19–21]. In contrast to the intra-columnar propagation of up-states, the layer-specific horizontal propagation of up-states has not been examined in naturally sleeping mammals [21–27].

Our understanding of the network properties underlying slow-waves and their propagation is limited and based almost exclusively on intra-cortical recordings from a few mammalian species. Interestingly, birds exhibit mammalian-like, homeostatically regulated EEG slow-waves during NREM sleep [28], even though the cytoarchitecture of the avian "cortex" differs from that of the mammalian neocortex [29]. During development, the dorsal part of the pallium gives rise to the neocortex in mammals and the hyperpallium in birds [30]. Although most of the hyperpallium is homologous to the primary visual cortex in mammals [29, 31, 32], it lacks the neocortical laminar cytoarchitecture consisting of pyramidal cells with apical dendrites spanning multiple layers. Instead, the hyperpallium is composed of small, densely packed stellate neurons [33] organized in "pseudo-layers", interconnected via axonal projections [29]. From dorsomedial to ventrolateral, the hyperpallium consists of the hyperpallium apicale (HA), interstitial nucleus of the HA (IHA), hyperpallium intercalatum (HI), and hyperpallium densocellulare (HD) [34]. Like layer 4 of the neocortex, IHA is the primary recipient of visual input from the dorsal part of the lateral geniculate nucleus (LGN, avian nucleus geniculatus lateralis pars dorsalis [GLd]) [35–38]; although HI and, to a lesser extent, HD also receive some input from the GLd [34]. (The exact boundary between IHA and HI is poorly defined in the posterior hyperpallium [39], and therefore will be referred to collectively as IHA/HI hereafter.) IHA/HI and, to a lesser extent, HD, project to HA, of which the superficial part is the main extra-telencephalic output region of the hyperpallium [34, 40, 41]. The presence of slow-waves in the avian hyperpallium—a "cortical" structure sharing some, but not all cytoarchitectonic traits with the mammalian neocortex—provides a unique opportunity to gain comparative insight into the mechanisms and functions of slow-waves and their propagation. Hence, in this study we characterized the spatiotemporal properties of slow-waves in the avian hyperpallium during natural NREM and REM sleep. In addition, we examined the hyperpallial and thalamic recordings for the existence of sleep spindles, which have not been detected in earlier EEG recordings in birds [42].

Materials and Methods

Experimental design

Animals

Nine adult pigeons (*Columba livia*; four females and five males) were used in this study. Birds were reared and housed in a breeding aviary. Preceding the start of the electrophysiological procedure, birds were taken from the colony and housed in a room with recording aviaries (12 h:12 h light:dark cycle, aviary dimensions: length = 2 m, width = 1 m, height = 2 m). All procedures were performed in accordance with German laws and regulations on animal experiments, and were approved by the Government of Upper Bavaria, according to the Tierschutzgesetz, approval number 55.2-1-54-2532-126-2013.

Surgery

Prior to surgery, birds received an injection of diazepam (2 mg/kg) into the breast muscle. Ten minutes later, they were anesthetized with isoflurane gas vaporized in oxygen (induction: 3%–4% and maintenance: 1.5%–3.5%). Subsequently, the bird's head was fixed in a custom-built stereotaxic frame (i.e. two ear bars and bill clamp). The head (i.e. the mouth bar) was angled downward 25° relative to the horizontal axis of the ear bar of the stereotaxic frame. The bird's body temperature was maintained around 40°C with a heat pad. Body temperature was checked continuously with a thermometer (Thermalert TH5, Physitemp Instruments Inc., Clifton, NJ) placed underneath the bird's abdomen. To prevent dehydration during the surgery, a subcutaneous injection of saline (0.7–0.9 mL NaCl 0.9% in sterile water) was administered into the neck. Prior to performing a midline incision, head feathers were clipped and Lidocaine gel (2%, as analgesia) was applied to the skin. An initial small window was made in the first layer of the skull to expose the bifurcation point of the midsagittal sinus, which served as a coordinate zero point. In the second skull layer, two small holes were made over the left and right side of the cerebellum for later insertion of the ground and reference wires. A second craniotomy was made on the right side, overlaying the probe insertion site in order to target either the posterior visual hyperpallium or the thalamus. Probe implants in the posterior visual hyperpallium ($N = 5$) were placed between 6800 and 7050 µm anterior, between 1250 and 1600 µm lateral, and in the thalamus ($N = 4$) between 6250 and 6400 µm anterior, between 2600 and 2900 µm lateral. Due to the use of a smaller size pigeon (Tippler) compared to the birds in

the Karten and Hodos atlas [39], these coordinates resulted in probe placements in areas histologically comparable with atlas coordinates A10.50 (hyperpallium; including the lower part of HA, IHA/HI, and the top part of HD) and A6.50 (thalamus, including the LGN; avian GLd; and the nucleus rotundus, a thalamic nucleus that is part of the tectofugal visual pathway [39, 43]; Figure 1A and Supplementary Figure S1). An incision was made in the dura for the coronal probe insertion. Preceding probe insertion, multiple small holes (dental acrylic anchor points) were drilled in the first layer of the skull surrounding the insertion side. In addition, the skull surrounding the holes and craniotomies was prepared using Clearfil SE Bond 2 (Kuraray Co., Ltd) for later dental acrylic attachment. The positioning of the probe was completed using a micromanipulator. The precise positioning of the probe depended on avoidance of blood vessels on top of the brain. The probe was slowly lowered, until all 32 channels were inside the brain (posterior visual hyperpallium: top row of electrode sites approximately 700 μm underneath brain surface and thalamus: top row approximately 8500 μm underneath the brain surface). After the probe was in position, the exposed brain and protruding probe shanks were covered using Kwik-Sil (World Precision Instruments). Next, the ground and reference wires were placed between the skull and the dura overlaying the cerebellum. Dental acrylic (Tetric EvoFlow, Ivoclar Vivadent) was used to secure the electrode and connector to the skull. Finally, the skin was sutured around the base of the dental acrylic. In addition, Lidocaine gel (as analgesia) was applied to the wound, and an intramuscular injection of meloxicam (2 mg/kg) and a subcutaneous injection of saline (0.7–0.9 mL) were administered, before letting the pigeon wake up from the anesthesia.

Natural sleep recordings

After the pigeon had fully awoken from the surgery, the wireless head stage (Multi Channel Systems, Reutlingen, Germany) was attached and the bird was brought back to the aviary. The birds quickly resumed normal behavior including feeding and flying to and from their perch. Recordings were made during the first night and at least 1 week later. Neuronal activity was recorded using 32-channel silicon-based multi-electrode probes (NeuroNexus Technologies, Ann Arbor, MI: hyperpallium, a4×8-5 mm-200-400-177 and thalamus, a2×16-10 mm-100-500-177) attached to a CM32 connector. The hyperpallium probe consisted of four parallel shanks (shank thickness, 15 μm) separated by 400 μm, each holding 8 recording sites (site surface, 177 μm^2) spaced 200 μm apart. The resulting matrix of 4 × 8 recording sites thus extended over 1200 × 1400 μm allowing for the simultaneous recordings of the lower part of HA, IHA/HI, and the top part of HD [39]. The thalamic probe consisted of two parallel shanks (shank thickness, 50 μm) separated by 500 μm, each holding 16 recording sites (site surface, 177 μm^2) spaced 100 μm apart. The resulting matrix of 2 × 16 recording sites thus extended over 500 × 1500 μm, allowing for simultaneous recording of the LGN (avian GLd) and the nucleus rotundus. For both probes, the 32 channels were referenced to a wire under the skull and over the cerebellum. The probe's Omnetics connector was attached to a wireless head stage with integrated amplifier (W32, 0.1 Hz–5 kHz bandwidth, 16 bits resolution, 5 kHz sampling rate per channel, 12.5 mV input voltage range; Multi Channel Systems, Reutlingen, Germany). The head stage was powered by a 900 mAh battery (LiPol Battery Co., Ltd) which was attached to the birds' back with a Velcro strip glued to trimmed feathers. The amplified and digitized signal was sent to a wireless receiver, which in turn was connected to the USB interface board and a data acquisition computer with MC_Rack software (Multi Channel Systems, Reutlingen, Germany). Before the start of each recording session, the battery was placed on the bird's back and attached to the head stage. Brain activity was recorded in naturally sleeping pigeons from lights off till lights on (i.e. 12 consecutive hours).

Diazepam injection

An additional experiment using diazepam was performed in an attempt to pharmacologically induce sleep spindles. First the birds (N = 3 hyperpallium implant and N = 3 thalamic implant) were habituated to sit and nap in a wooden recording chamber (length = 79 cm, width = 60 cm, height = 60 cm) [44] for 2 h in the morning (starting 2 h after lights on) on 2 consecutive days. The experiment consisted of two experimental days separated by 48 h. Using a balanced design, each bird was randomly assigned to a treatment order, either receiving a diazepam injection on the first day and a saline injection on the third day or vice versa. On the morning of the experiment, the bird was equipped with a transmitter and battery, and placed in the recording chamber with water and food. Brain activity was recorded for 2 h before diazepam (7 mg/kg) or saline (equal volume to the diazepam injection) was injected into the breast muscle. The bird was subsequently placed back into the chamber and recorded for another 3 h (i.e. until the overt behavioral effects of diazepam had worn off). The birds were video recorded throughout the experiments.

Anatomy

Prior to implantation, the electrode probes were coated with the fluorescent dye DiI (DiIC 18(3), Invitrogen) for anatomical registration with histological sections. At the end of the study, the brain was removed and frozen for histology to determine probe placement. Frozen brains were cut into 20 μm serial coronal sections using a freezing microtome and mounted on glass slides. Subsequently, 4',6-diamidino-2-phenylindole (DAPI) and Nissl staining was applied. Fluorescence microscopy (Leica) was used to verify probe location in all birds.

Analysis

Natural sleep scoring

For each bird, a full night recording, at least 1 week post-surgery, was analyzed. From this recording, 2 h of "early" night sleep (i.e. 1 h after lights off) and 2 h "late" night sleep (i.e. 2 h before lights on) was extracted. Within these recordings one representative channel, near the center of the array, was chosen for sleep scoring. Raw data of the selected channel were offline low-pass filtered at 100 Hz and down-sampled at 200 Hz using MC_Rack software (Multi Channel Systems, Reutlingen, Germany). Subsequently, sleep stages were manually scored by visual inspection of the LFP signal using Somnologica (Embla Sleep Diagnostics) and the video recordings, in order to differentiate sleep stages and exclude (movement) artifacts. Rather than using scoring epochs, sleep stages were scored from the start until the end of each bout of each state. In both the hyperpallial and thalamic recordings, wake was characterized by low-amplitude, high-frequency LFP signals in combination with waking behaviors; NREM sleep by high-amplitude, low-frequency LFP signals and immobility; and

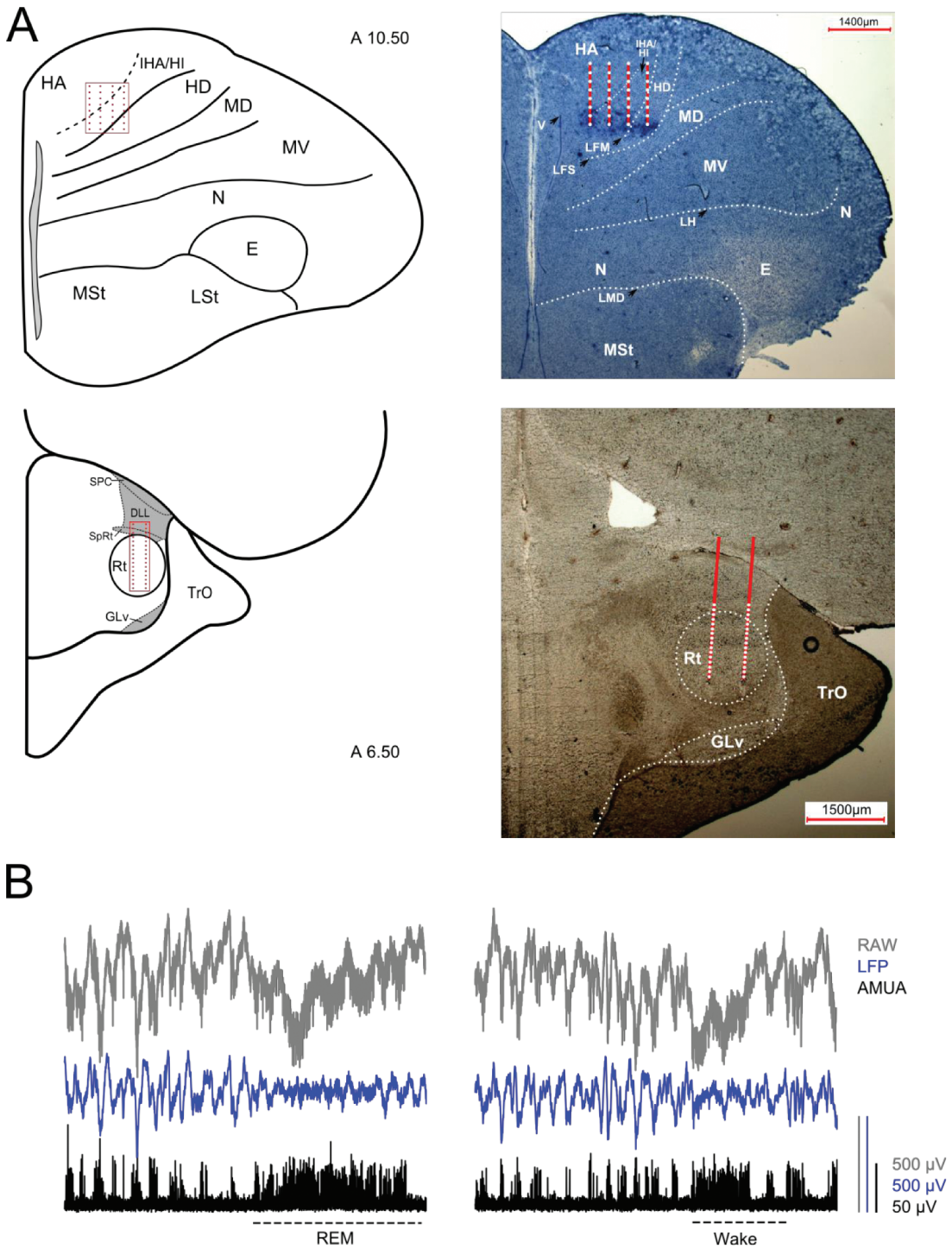

Figure 1. Recording method: (**A**) Schematic and histological example of the location of the 32-channel silicon electrode probe. Probes were inserted horizontally in either the hyperpallium (*N* = 5 birds) or the thalamus (*N* = 4 birds). The exact probe location for each bird is depicted in Supplementary Figure S1. The orientation of the electrode grid (red) is always depicted with the medial side to the left and the surface of the brain on top. The hyperpallium (top) primarily receives input from the GLd (mammalian LGN) to the interstitial part of HA and the hyperpallium intercalatum (IHA/HI, collectively). The underlying hyperpallium densocellulare (HD) receives relatively little input from the GLd. The hyperpallium overlies and is interconnected with the dorsal and ventral mesopallium (MD/MV) and nidopallium (N). The avian thalamus (bottom) includes the nucleus rotundus (Rt), which projects to the entopallium (E), and the GLd (gray) of which several parts project to IHA/HI. (**B**) Raw signals (gray) were filtered to a signal containing local field potentials (LFP, 1.5–200 Hz; blue) and to a signal containing multiunit action potentials (MUA, high-pass filtered at 350 Hz). In addition, the MUA signal was rectified and decimated to obtain an analogue multiunit activity (AMUA; black) signal. The top panel shows an NREM sleep episode, with increased AMUA occurring during negative waves corresponding to up-states, followed by REM sleep. The right panel shows an example of NREM sleep followed by wake. Both REM sleep and wake states show a continuous action potential firing pattern compared to NREM sleep. DLL = nucleus dorsolateralis anterior thalami pars lateralis, GLv = nucleus geniculatus lateralis pars ventralis, HA = hyperpallium apicale, LFM = lamina frontalis suprema, LFS = lamina frontalis superior, LH = lamina hyperstriatica, LMD = lamina medullaris dorsalis, LSt = striatum laterale, MSt = striatum mediale, SPC = nucleus superficialis parvocellularis, SpRt = nucleus suprarotundus, TrO = tractus opticus.

REM sleep by low-amplitude, high-frequency LFP activity in combination with REM sleep behaviors (e.g. eye closure and head drops). In addition, for two birds, the same scoring procedure was performed for the recording of the first night after surgery, to assess the development of very slow artifacts encountered in later recordings. Power below 1.5 Hz increased during the first postoperative week and, unlike higher frequency slow-waves (>2 Hz), had an irregular distribution across the array. Activity below 1.5 Hz likely reflects an artifact resulting from the development of gliosis around the electrodes [45]. To remove this activity, a 1.5 Hz high-pass filter was applied to the signals.

Filtering

All electrophysiological raw data were filtered and analyzed in Python, version 2.7, using signal analysis and array computation functionality of the scientific computing packages NumPy [46], version 1.10.3, and SciPy [47], version 0.17.0. Raw recordings were band-pass filtered (finite impulse response filter) from 1.5 to 200 Hz to yield LFP signals, and high-pass filtered at 350 Hz to yield action potential activity. Action potential signals were subsequently rectified, resulting in an analog multiunit activity (AMUA) signal that reflects the level of multiunit action potential firing in the vicinity of the electrode site (Figure 1B). Signals were then decimated to a sampling rate of 1000 Hz to facilitate the calculation of correlation coefficients and visualization.

Slow-wave analysis

The following analyses were performed on the filtered signals (excluding [movement] artifacts and broken electrodes sites) following, with some exceptions, the method previously described in Beckers et al. [48]. In addition, as no differences were found between signals recorded from male and female pigeons, birds implanted in the same region (i.e. hyperpallium vs. thalamus) were grouped together for the following analyses.

Initial inspection of the LFP and AMUA signal was performed by creating waveform plots of each 2 h recording including color coding of each sleep stage. To examine whether the LFP signal during each sleep stages on a specific site coincided with spiking activity on the same channel, the mean correlation coefficient between LFP and a smoothed (low-pass filtered at 1000 Hz) version of the AMUA signal was calculated, when sites showed strong action potentials (Figure 1B).

Temporospatial propagation of LFP slow-waves across the recording electrode matrix was quantified to examine traveling wave activity [48]. In short, at intervals of 1 ms, LFP waves in the electrode grid that were stronger (i.e. more negative) than the threshold criterion of −125 mV were identified, and the changes of their spatial mean in time were tracked. The median number of traveling wave "trajectories" that were found in the 2 h hyperpallium recordings was 14 659 (range: 6770–25 691). The overall periodicity of LFP during NREM sleep was determined for each 2 h recording, based on the lag of the first positive peak at t greater than 0 in the mean autocorrelation function. Although the LFP signal during NREM sleep in the thalamus showed clear slow-waves, the overall lower amplitude of the slow-waves and the spatial configuration of recording sites (relatively large distance between the two probe shanks) made the recording data unsuitable for 2D wave propagation analysis (data not shown).

Videos illustrating the slow-wave patterns were rendered from the band-pass filtered LFP signal (1.5–200 Hz) in either real-time or slowed down 25× and 50×, in order to capture individual travelling patterns.

State-specific spectral analysis

Power spectral density (PSD) was calculated (using Welch's method; 0.5 Hz bin size) for all episodes of NREM/REM/wake (duration >4 sec, without wake interruptions) within each 2 h sleep recording. Then mean PSD for each state was calculated for each recording site for each bird. In addition, mean slow-wave activity (SWA; power in 1.5–4.5 Hz band) was calculated for NREM and REM sleep for each bird.

Statistics

Statistical analysis was performed in R (version 3.4.4). Unless noted otherwise, all values are the mean ± *SD*.

Results

We recorded electrical activity from the pigeons' visual hyperpallium and thalamus, including parts of the dorsal part of the LGN and nucleus rotundus, during natural NREM and REM sleep, using a high-density electrode array connected to a telemetric system (Figure 1).

NREM sleep slow-waves

During NREM sleep, slow-waves occurred across all LFP recording sites, but had the highest amplitude in electrode sites corresponding to IHA/HI based on stereotaxic coordinates and histology (Figure 2A and B). The hyperpallial slow-waves had a periodicity of 2.2 Hz ± 0.09 Hz (N = 4 birds; Figure 2C). In all birds, slow-waves propagate through the hyperpallium during natural NREM sleep. This is most readily apparent when slow-wave LFPs are plotted in a time series of images where pixels represent electrode sites and electrical potential is coded in color (Figures 2D and 3, Supplementary Figure S2 and Supplementary Video S1). Moreover, tracing the trajectories of the center of gravity of propagating slow-waves shows that slow-waves often occur first along the diagonal of the recording plane (Figure 2E and Supplementary Figure S3), corresponding to IHA/HI. In addition, the net movement of each slow-wave across the plane of the electrode grid was expressed as a mean vector (Figure 2E and Supplementary Figure S4). Group mean vectors for both positive and negative slow-waves have significantly nonrandom directions (Rayleigh-tests; $p < 0.001$) in every recording (N = 10 2 h recordings from 4 birds), with an overall tendency for slow-waves to travel toward the surface of the brain (Supplementary Figures S3 and S4). Overall, slow-waves primarily propagate within IHA/HI, but they also propagate to the overlying lower part of HA and to a lesser extent to the underlying top part of HD. In rare cases, slow-waves occurred first or exclusively in regions other than IHA/HI (Figure 3; e.g. frame 210).

AMUA was only present shortly after the implantation. Although AMUA was visible on several recording sites, only two electrode sites in two birds showed AMUA that was strongly differentiated from the background activity. Nonetheless, in these recordings and electrode sites, there is a clear relationship

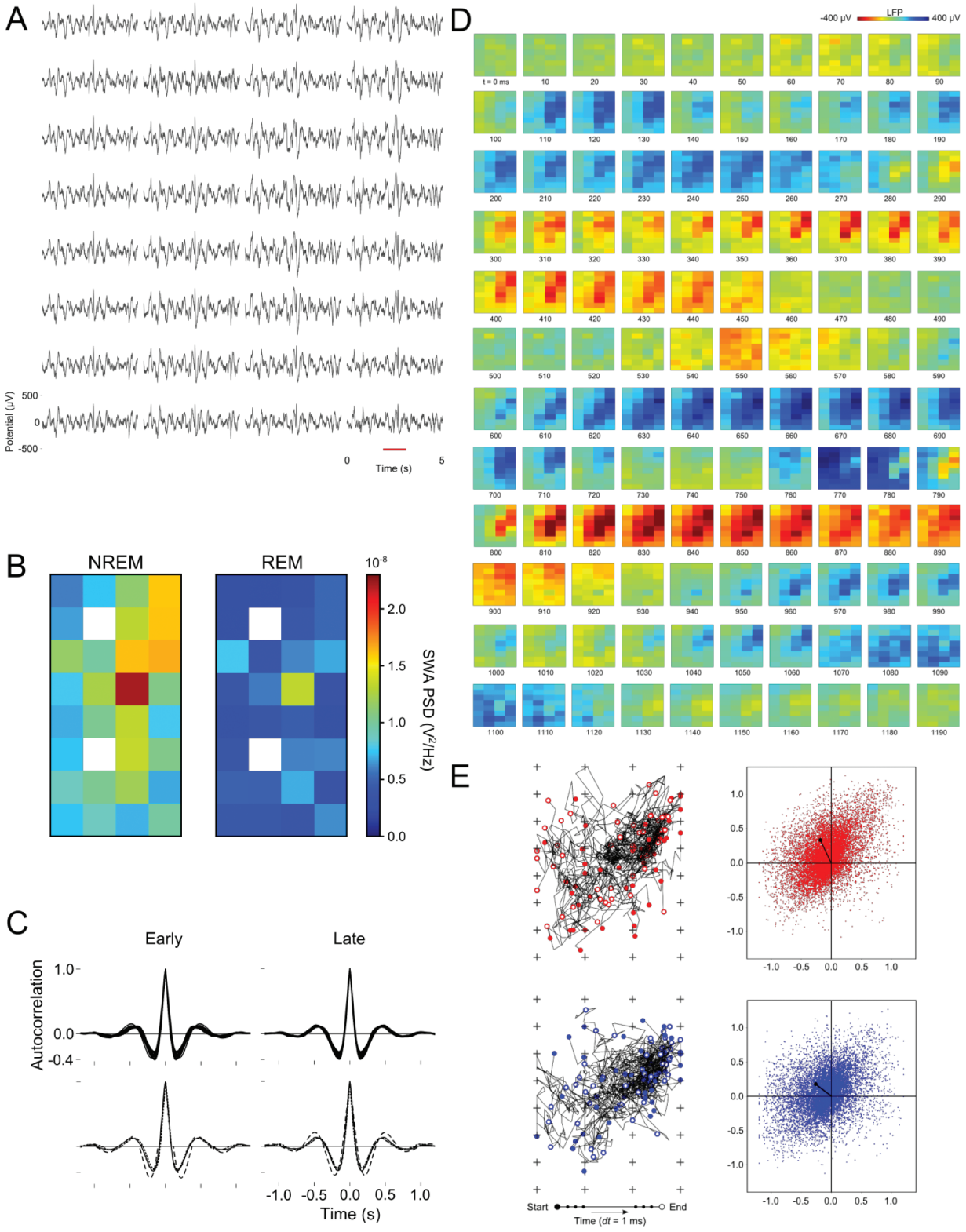

Figure 2. Slow-waves in the hyperpallium: (**A**) Five-second example of LFPs recorded on the 4 × 8 grid of electrode sites, showing a global distribution of oscillations during natural NREM sleep (recorded the night after implantation). (**B**) Mean slow-wave activity (SWA; 1.5–4.5 Hz; *N* = 4 birds) over all episodes of NREM and REM sleep. SWA during NREM sleep is the highest in the diagonal of the recording array. The same part also shows the highest decrease in SWA during REM sleep. (**C**) Average autocorrelation of all 32 channels of one bird (top) and of one channel (from the middle of the array) for each bird (*N* = 4; bottom, different dotted lines correspond to different birds) comparing early and late night NREM sleep. The mean lag between the first positive peak (*t* = 0) and the second positive peak is on average 460 ms, indicating that the LFP waves on the same electrode site follow a periodicity of approximately 2.2 Hz. (**D**) Red underlined episode of Figure 2A is visualized in a sequence of image plots where pixels represent electrode sites and electrical potential is coded in color. (**E**) Wave trajectories along the array (left; *N* = 50 random waves; plus sign depicts electrode sites). Net wave propagation (right) was calculated for every LFP wave in a 2 h recording of the same bird; shown are negative (red dots; i.e. up-state) and positive waves (blue dots; i.e. down-state), and mean propagation direction (black dot).

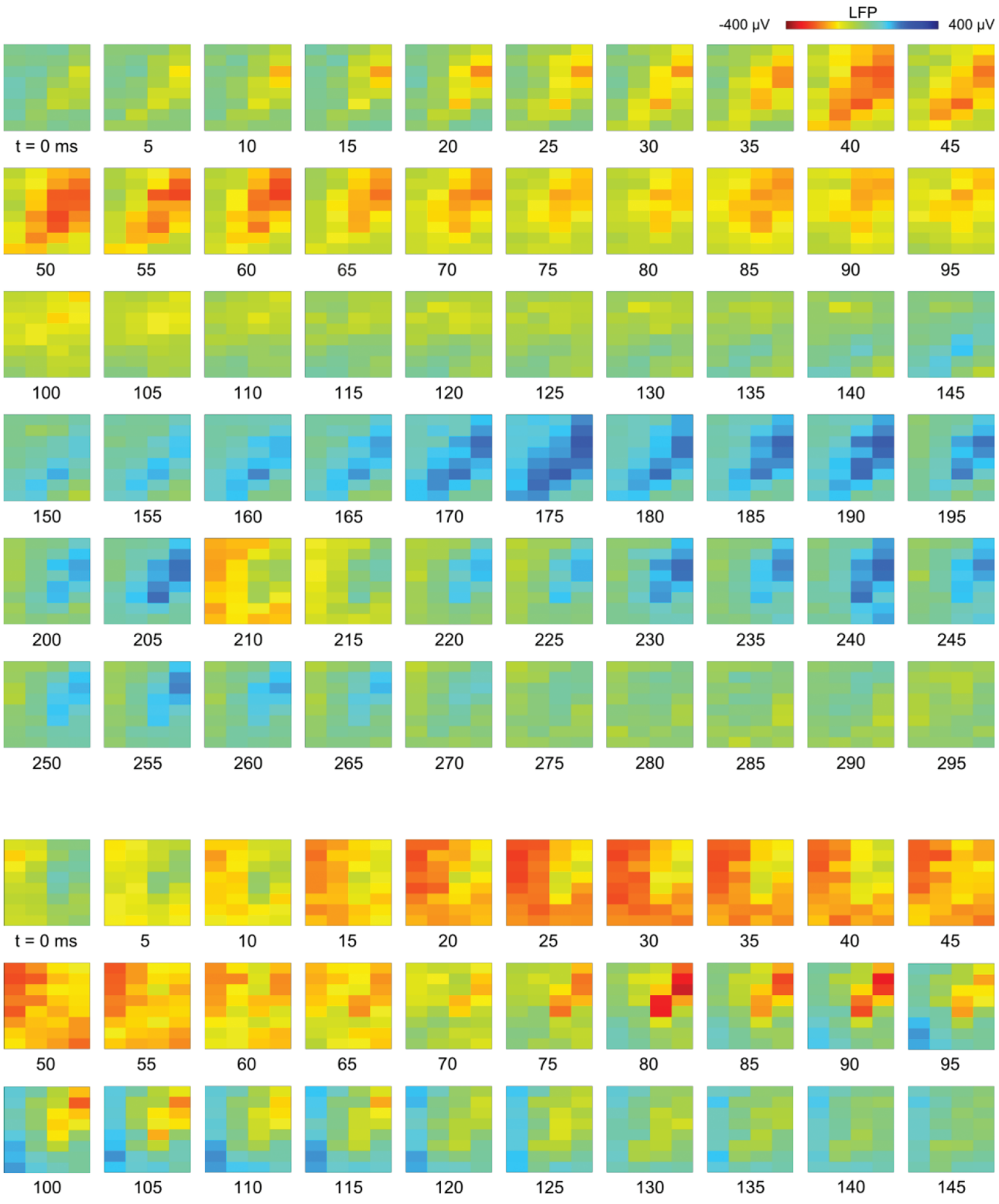

Figure 3. Examples of propagating slow-waves: two more examples from the same recording as Figure 2D depicting different propagation patterns. LFP activity often initiates at different points along the diagonal of the recording plane, corresponding to IHA/HI, and propagates mostly within the diagonal. Rare activity initiated outside of the electrode array propagates across HA and HD, but is often not found on the diagonal sites in these cases.

between unit activity and LFP slow-waves during NREM sleep, with increased AMUA occurring during negative waves, presumably corresponding to up-states (Figure 1B). The mean correlation coefficient between LFP and AMUA in full recordings of these sites during "early" and "late" NREM sleep is –0.45 and –0.42, respectively (N = 2 birds). This is similar to the correlation between LFP and AMUA of slow-waves in anesthetized zebra finches [48]. In addition, this high correlation of sites that had

strong AMUA shows that local neurons are part of the system that generates the LFP signal we observed.

NREM sleep spindles

NREM sleep spindles were not detected during visual inspection of the waveform and spectrogram plots for all NREM sleep episodes in each 2 h recording. In addition, PSD analysis of LFP did not reveal a distinct peak in power between 6 and 15 Hz, corresponding to spindles in mammals [49], in any of the hyperpallial layers during early or late NREM sleep (Figure 4). In fact, the only distinct power peaks correspond to SWA. Also, no sleep spindles were detected in the dorsal part of the LGN, which projects to IHA/HI, during NREM sleep. Spindles were also not detected in the nucleus rotundus (Figure 4). In addition, although diazepam induced instability and NREM sleep (total time spent in NREM sleep during diazepam treatment increased by 1.8–5.5 times in the hyperpallium (N = 3 birds) and 1.9–2.1 times in the thalamic (N = 3 birds) recordings when compared to the saline treatment), we did not find an increase in spindle power, in comparison to spontaneous NREM sleep, in the hyperpallium or the thalamus (Figure 5). Nonetheless, diazepam augmented SWA in all of the three birds with a hyperpallial implant, but suppressed SWA in only one of the three birds with a thalamic implant (Figure 5).

REM sleep

Although the percentage of time spent in NREM sleep decreased only slightly overnight ("early" vs. "late" night:

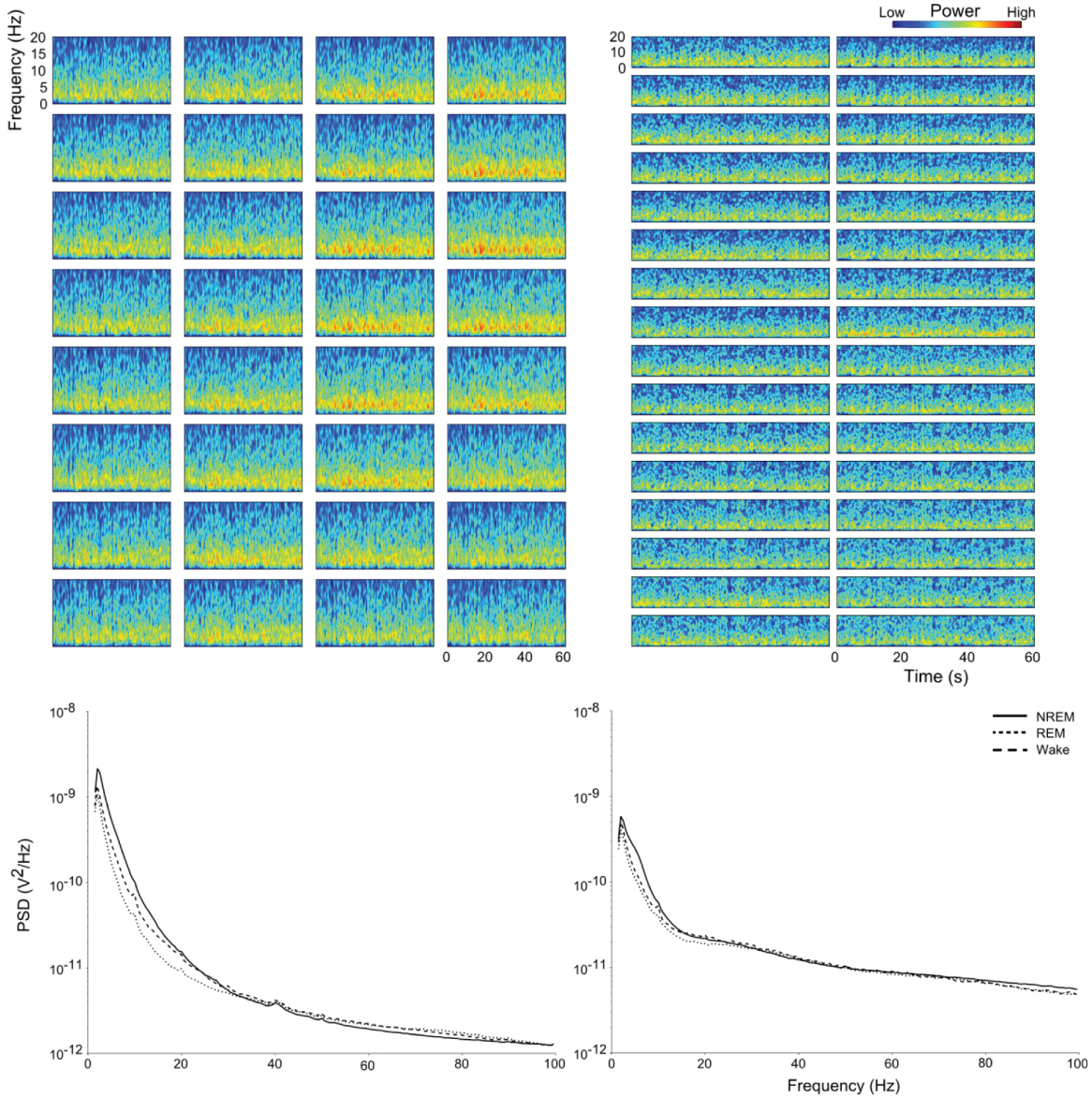

Figure 4. Absence of sleep spindles in the hyperpallium and thalamus during NREM sleep: Both hyperpallium (top left) and thalamus (top right) example spectrograms lack an elevated power band in the sleep spindle range (6–15 Hz). Mean power spectral density (PSD) over all birds and all episodes of NREM sleep, REM sleep, and wake, separately for hyperpallium (bottom left) and thalamus (bottom right) recordings. Each state shows a power frequency distribution typical for pigeon sleep [44]; however, no bump in the spindle frequency range is visible during NREM sleep in either of the two brain regions. This is consistent with visual inspection of individual recordings sites and birds (Supplementary Figure S5).

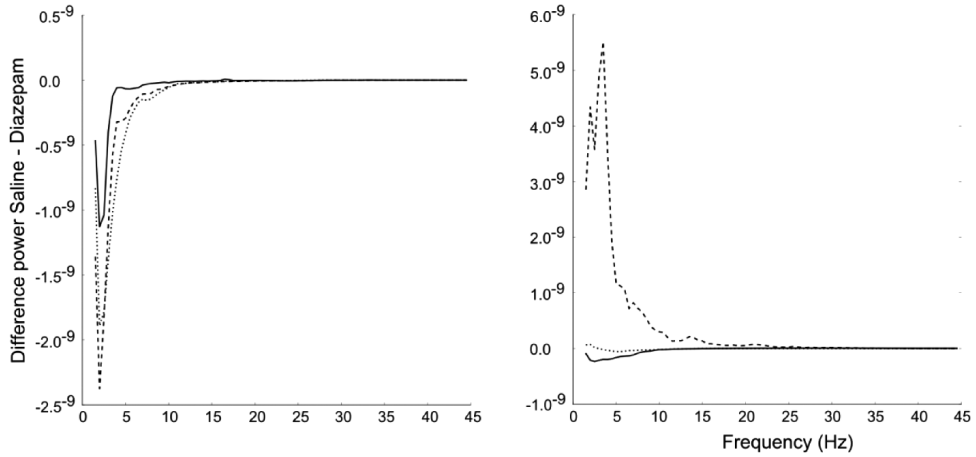

Figure 5. Effect of diazepam on LFP spectral power: For each bird, the PSD of diazepam treatment was subtracted from the PSD of the saline treatment to visualize the effect of diazepam on the LFP spectral power in the slow-wave and spindle range in the hyperpallium (left) and thalamus (right). Different line styles reflect data from different birds.

hyperpallium = 79.9% vs. 74.5% [N = 5 birds], thalamus = 78.3% vs. 76.7% [N = 4 birds] time spent in NREM sleep), the percentage of time spent in REM sleep increased as the night progressed ("early" vs. "late" night: hyperpallium = 7.0% vs. 14.2%, thalamus = 10.2% vs. 15.7% time spend in REM sleep), which is consistent with results from previous studies on sleep in pigeons [44]. REM sleep episodes were typically short ("early" vs. "late" night: hyperpallium [4.8 ± 2.7 s vs. 7.5 ± 5.4 s], thalamus [5.1 ± 3.1 s vs. 5.8 s ± 7.3 s]).

During REM sleep, action potential firing (AMUA) in the hyperpallium became visually more continuous relative to preceding NREM sleep and was similar to that during wakefulness (Figure 1B). SWA decreased across all recording sites, with the greatest reduction in SWA occurring in IHA/HI (Figure 2B), the region with the greatest SWA during NREM sleep. In addition, in two birds, visual inspection of spectrograms and power spectral analysis revealed an increase of fast gamma rhythm (approximately 70–90 Hz) during both early and late night REM sleep episodes occurring in IHA/HI (Figure 6). Gamma was not present in all REM sleep episodes or, when it did occur, throughout an entire episode. The bursts of gamma could occur at any point (early, middle or late) within a REM sleep episode.

Discussion

Previously, our understanding of how brain activity changes during NREM and REM sleep in birds was primarily based on EEG recordings from the hyperpallium. These studies revealed several similarities with mammalian sleep (e.g. homeostatically regulated slow-waves during NREM sleep and EEG activation during REM sleep), as well as some differences, such as the absence of thalamocortical spindles [42, 44, 50, 51]. Using intra-"cortical" high-density electrode arrays in naturally sleeping pigeons, we characterized the spatiotemporal properties of slow-waves in the avian hyperpallium during NREM and REM sleep.

Traveling slow-waves during NREM sleep

Our intra-"cortical" recordings of pigeons revealed that slow-waves propagate through the hyperpallium during natural NREM sleep. Interestingly, whereas slow-wave up-states in the mammalian neocortex usually appear first in the thalamo-recipient layer 5 and then propagate vertically within a column to layer 4 and the supragranular layers [19–21], slow-waves in the hyperpallium predominantly initiate in IHA/HI, the avian analog of the neocortical layer 4, and then propagate to the overlaying HA, a "pseudo-layer" of which the superficial part is thought to be analogous to layer 5 of the mammalian neocortex based on its similar extra-telencephalic projections to the thalamus, striatum, and brainstem [29]. Nonetheless, in both mammals and birds initiation of slow-waves is largely thalamo-recipient layer specific. In addition, the propagation of slow-waves parallel to the hyperpallial pseudo-layers also occurs primarily within IHA/HI. Here, a direct comparison with the horizontal propagation of slow-waves in the mammalian neocortex is hindered by the absence of comparable data from naturally sleeping mammals. Nonetheless, most slice and anesthesia studies of the neocortex suggest that layer 5 plays a dominant role in the horizontal propagation of slow-waves [21–24, 26, 27, 52, 53]. In general, propagating slow-waves in the hyperpallium may be involved in functions attributed to slow-waves propagating through the mammalian neocortex. These include the successive reactivation and consolidation of recent memory traces [7] and/or their relocation and incorporation with older memories [10].

Absence of sleep spindles during NREM sleep

Sleep spindles were not found in the avian visual hyperpallium or in the thalamus during NREM sleep. Furthermore, diazepam, a benzodiazepine known to increase activity in the spindle frequency range in humans [54] and rats [55, 56], did not change spindle frequency power in the hyperpallium or thalamus, even though the dose used induced locomotor instability followed by NREM sleep. Interestingly, although diazepam did not increase power in the spindle range, it did increase SWA in the hyperpallium, a response opposite to that observed in the neocortex [57–59]. Our results suggest that, at least within the visual hyperpallium, functions attributed to spindles in mammals, such as memory consolidation, might occur via different mechanisms in birds [42]. Additional studies are

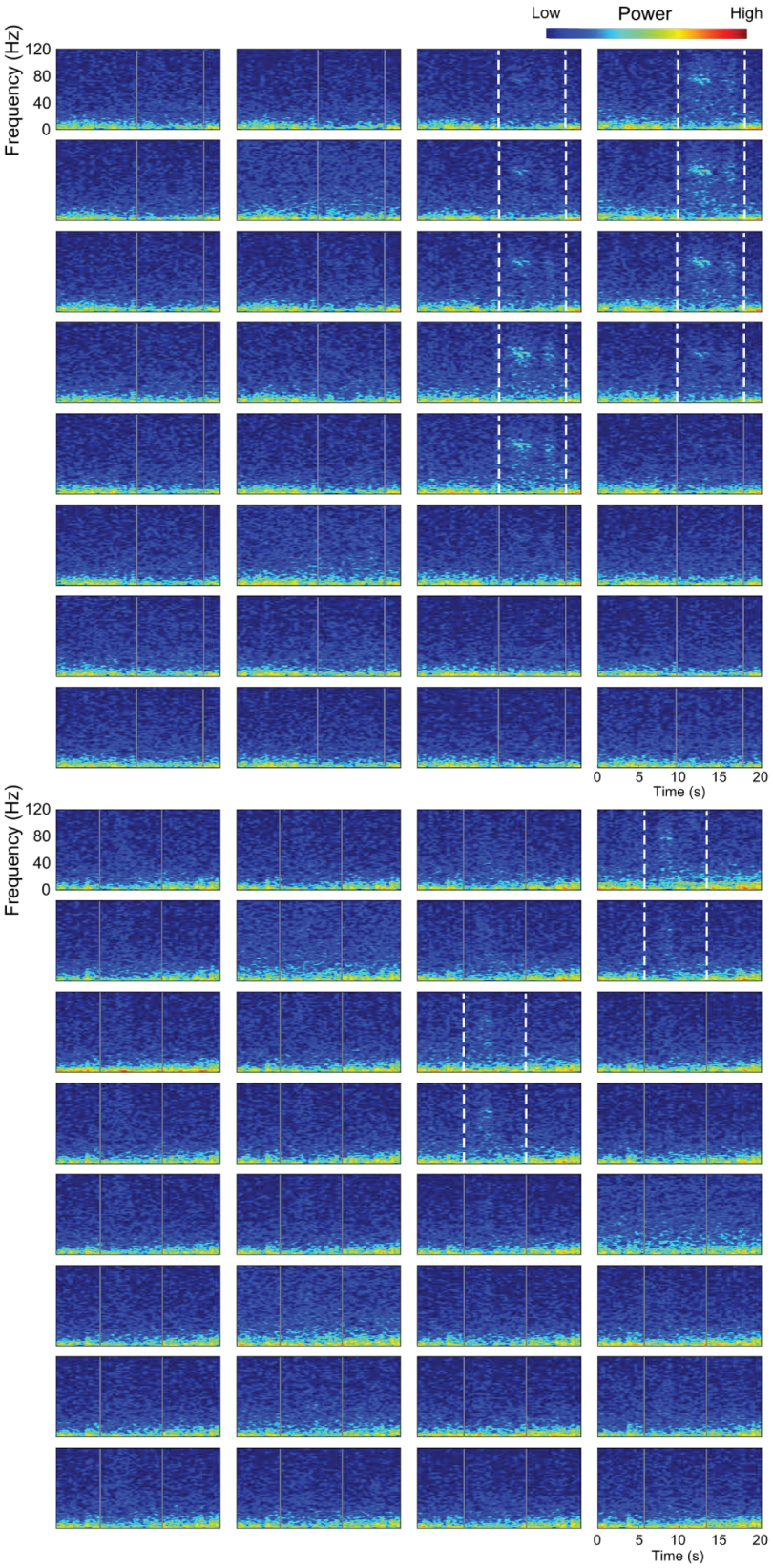

Figure 6. Fast gamma during REM sleep: Pronounced examples from two different birds (top vs. bottom grid) of fast gamma oscillations (around 70–90 Hz) on the diagonal recording sites, corresponding to the thalamo-recipient layer IHA/HI, during a REM sleep episode (in-between two NREM sleep episodes) indicated with the white dashed lines. Each panel represents an electrode site of the 4×8 grid. Electrode sites, during the same REM episode, but without fast gamma are indicated with continuous gray lines.

needed to determine whether sleep spindles occur in other regions of the avian brain.

Avian REM sleep

As in mammals [60], during REM sleep, AMUA in the hyperpallium increased relative to preceding NREM sleep and SWA decreased across all hyperpallial recording sites. However, the largest decrease in SWA occurred in IHA/HI, the region with the greatest SWA during NREM sleep. Interestingly, this is opposite to the pattern observed during REM sleep in mice wherein slow-waves persist in layer 4 of primary sensory cortices, including the primary visual cortex [5], the mammalian analogue of the visual hyperpallium. Although it is unknown whether these divergent findings in pigeons and mice are representative of all birds and mammals, respectively, the results from pigeons indicate that the occurrence of slow-waves in primary sensory input layers is not a universal phenomenon in animals with REM sleep.

In addition, in two birds, distinct bursts of gamma with peak power around 70–90 Hz occurred exclusively during episodes of REM sleep. Interestingly, these bursts were restricted to IHA/HI, where SWA was the greatest during NREM sleep. Previous studies of the sleep-related EEG power spectrum in birds only focused on frequencies less than 25–30 Hz [28, 44, 61, 62] or less than 50–55 Hz [51, 63]; in the later, gamma (30–55 Hz) was higher in REM sleep in adult zebra finches (*Taeniopygia guttata* [51]), but not in barn owl nestlings (*Tyto alba* [63]). This difference may be related to the species, age, or recording methods employed (epidural versus subcutaneous electrodes, respectively). In addition, if gamma is primarily present in IHA/HI, the distance between the EEG electrodes and this region might explain this difference. The fact that only two of the five hyperpallial recordings in the present study showed gamma bursts also suggests that there is spatial heterogeneity in the production of gamma within the hyperpallium. Additional research is needed to determine the exact region generating gamma and its functional relationship to gamma reported during REM sleep in rodents [64–66] and humans [67, 68].

Implications and future perspectives

Collectively, our intra-"cortical" recordings of naturally sleeping pigeons revealed both invariant and variant traits between birds and mammals. Although slow-waves propagate through the hyperpallium and neocortex during NREM sleep, the layer-specific contribution to propagation differed between mammals and birds. Despite this difference, in both cases the leading layer is known to receive thalamic input, suggesting a common role for the thalamus in the genesis of slow-waves. Although slow-waves were also detected in the thalamic nuclei examined, dual thalamic/hyperpallial recordings are needed to further characterize thalamocortical interactions in birds. Interestingly, unlike mammals, spindles were not detected in the hyperpallium or thalamus of pigeons, even following administration of a pharmacological compound known to augment spindling in mammals. The absence of spindles seemingly poses a challenge for the mammalian-based hypothesis that the phase-locking of spindles with neocortical slow-waves and hippocampal SWRs [12] plays a role in the systems-level processing of hippocampal memories, involving the "transfer" of information initially encoded in the hippocampus to the neocortex for long-term storage and integration with preexisting information [7, 10, 69, 70]. However, limited interconnectivity between the avian hippocampus and brain regions analogous to the neocortex [41], the absence of evidence for memory transfer out of the avian hippocampus, and the apparent absence of hippocampal SWRs in birds, all suggest that the avian and mammalian hippocampi process information in a different manner [42, 71]. In this respect, the absence of spindles in birds is consistent with their proposed role in processing hippocampal information in mammals [13, 72, 73]. Nonetheless, the presence of propagating slow-waves in birds, despite the lack of spindles and SWRs, indicates that slow-waves also likely serve functions unrelated to hippocampal memory transfer in birds and mammals. Notably, the fact that SWA is homeostatically regulated in a local, use-dependent manner in mammals and birds [28, 74, 75] suggests that slow-waves play a role in cellular and synaptic maintenance [8, 76] and/or the processing of information on a local scale [7, 74].

Finally, it is important to note that as our study only tapped into small portions of the avian brain, and it is conceivable that other regions developmentally and functionally homologous to portions of the neocortex might exhibit patterns of brain activity unlike those described in the hyperpallium. In the future, it will also be important to examine activity throughout the thalamus, including the thalamic reticular nucleus, which is involved in the genesis of mammalian spindles via the thalamocortical loop [77–79]. Although thalamocortical loops exist in birds, including reciprocal projections between the hyperpallium and thalamus [35, 80–83], their influence over thalamic activity has not been examined. Finally, a systems-level approach that simultaneously taps into multiple regions, including all "pseudo-layers" of the hyperpallium, the thalamus, and the hippocampus, is needed to determine if and how activity in the avian brain coordinates the processing of information across regions and the extent to which this differs from mammals [84]. This comparative approach holds the promise of revealing overriding principles that might not be readily apparent using a strictly mammalian approach to understanding the functions of sleep-related brain activity.

Supplementary material

Supplementary material is available at *SLEEP* online.

Authors' Contributions

J.vdM., G.J.L.B., and N.C.R. designed research; J.vdM. and D.M-G. performed research; J.vdM., D.M-G., G.J.L.B., and N.C.R. analyzed data; and J.vdM., G.J.L.B., and N.C.R. wrote the article.

Acknowledgments

We thank Manfred Gahr for providing laboratory facilities and equipment, Susanne Seltmann for help with the surgical procedure, and Martina Oltrogge for technical assistance. J.vdM. is a member of the International Max Planck Research School for Organismal Biology.

Funding

This study was supported by the Max Planck Society (J.vdM., D.M-G., and N.C.R.) and by a Marie Curie Intra European Fellowship within the 7th European Community Framework Programme to G.J.L.B. G.J.L.B. is part of the Consortium on Individual Development (CID), which is funded through the Gravitation Program of the Dutch Ministry of Education, Culture, and Science and the Netherlands Organization for Scientific Research (NWO; grant number 024.001.003).

Conflict of interest statement. None declared.

References

1. Steriade M, *et al*. A novel slow (< 1 Hz) oscillation of neocortical neurons in vivo: depolarizing and hyperpolarizing components. *J Neurosci*. 1993;**13**(8):3252–3265.
2. Massimini M, *et al*. The sleep slow oscillation as a traveling wave. *J Neurosci*. 2004;**24**(31):6862–6870.
3. Murphy M, *et al*. Source modeling sleep slow waves. *Proc Natl Acad Sci USA*. 2009;**106**:1608–1613.
4. Nir Y, *et al*. Regional slow waves and spindles in human sleep. *Neuron*. 2011;**70**(1):153–169.
5. Funk CM, *et al*. Local slow waves in superficial layers of primary cortical areas during REM sleep. *Curr Biol*. 2016;**26**(3):396–403.
6. Muller L, *et al*. Cortical travelling waves: mechanisms and computational principles. *Nat Rev Neurosci*. 2018;**19**(5):255–268.
7. Chauvette S, *et al*. Sleep oscillations in the thalamocortical system induce long-term neuronal plasticity. *Neuron*. 2012;**75**(6):1105–1113.
8. Tononi G, *et al*. Sleep and the price of plasticity: from synaptic and cellular homeostasis to memory consolidation and integration. *Neuron*. 2014;**81**(1):12–34.
9. Colgin LL, *et al*. Gamma oscillations in the hippocampus. *Physiology (Bethesda)*. 2010;**25**(5):319–329.
10. Diekelmann S, *et al*. The memory function of sleep. *Nat Rev Neurosci*. 2010;**11**(2):114–126.
11. Born J, *et al*. System consolidation of memory during sleep. *Psychol Res*. 2012;**76**:192–203.
12. Staresina BP, *et al*. Hierarchical nesting of slow oscillations, spindles and ripples in the human hippocampus during sleep. *Nat Neurosci*. 2015;**18**(11):1679–1686.
13. Latchoumane C-FV, *et al*. Thalamic spindles promote memory formation during sleep through triple phase-locking of cortical, thalamic, and hippocampal rhythms. *Neuron*. 2017;**95**:424–35.e6.
14. Ermentrout GB, *et al*. Traveling electrical waves in cortex. *Neuron*. 2001;**29**:33–44.
15. Caporale N, *et al*. Spike timing-dependent plasticity: a Hebbian learning rule. *Annu Rev Neurosci*. 2008;**31**:25–46.
16. Crunelli V, *et al*. The slow (< 1 Hz) rhythm of non-REM sleep: a dialogue between three cardinal oscillators. *Nat Neurosci*. 2010;**13**:10–18.
17. Timofeev I, *et al*. Thalamocortical oscillations: local control of EEG slow waves. *Curr Top Med Chem*. 2011;**11**(19):2457–2471.
18. Lemieux M, *et al*. The impact of cortical deafferentation on the neocortical slow oscillation. *J Neurosci*. 2014;**34**(16):5689–5703.
19. Chauvette S, *et al*. Origin of active states in local neocortical networks during slow sleep oscillation. *Cereb Cortex*. 2010;**20**(11):2660–2674
20. Constantinople CM, *et al*. Deep cortical layers are activated directly by thalamus. *Science*. 2013;**340**(6140):1591–1594.
21. Capone C, *et al*. Slow waves in cortical slices: how spontaneous activity is shaped by laminar structure. *Cereb Cortex*. 2017:1–17. doi:10.1093/cercor/bhx326
22. Sanchez-Vives MV, *et al*. Cellular and network mechanisms of rhythmic recurrent activity in neocortex. *Nat Neurosci*. 2000;**3**(10):1027–1034.
23. Luczak A, *et al*. Sequential structure of neocortical spontaneous activity *in vivo*. *Proc Natl Acad Sci USA*. 2007;**104**:347–352.
24. Sakata S, *et al*. Laminar structure of spontaneous and sensory-evoked population activity in auditory cortex. *Neuron*. 2009;**64**(3):404–418.
25. Chauvette S, *et al*. Properties of slow oscillation during slow-wave sleep and anesthesia in cats. *J Neurosci*. 2011;**31**:14998–5008.
26. Wester JC, *et al*. Columnar interactions determine horizontal propagation of recurrent network activity in neocortex. *J Neurosci*. 2012;**32**(16):5454–5471.
27. Reyes-Puerta V, *et al*. Laminar and columnar structure of sensory-evoked multineuronal spike sequences in adult rat barrel cortex in vivo. *Cereb Cortex*. 2015;**25**(8):2001–2021.
28. Lesku JA, *et al*. Local sleep homeostasis in the avian brain: convergence of sleep function in mammals and birds? *Proc Biol Sci*. 2011;**278**:2419–2428.
29. Medina L, *et al*. Do birds possess homologues of mammalian primary visual, somatosensory and motor cortices? *Trends Neurosci*. 2000;**23**(1):1–12.
30. Puelles L, *et al*. The pallium in reptiles and birds in the light of the updated tetrapartite pallium model. In: Striedter G, ed. *Evolution of Nervous Systems*, 2nd ed. San Diego, CA: Academic Press/Elsevier; 2017.
31. Reiner A, *et al*. Avian Brain Nomenclature Forum. Revised nomenclature for avian telencephalon and some related brainstem nuclei. *J Comp Neurol*. 2004;**473**(3):377–414.
32. Jarvis ED, *et al*. Avian brains and a new understanding of vertebrate brain evolution. *Nat Rev Neurosci*. 2005;**6**:151–159.
33. Olkowicz S, *et al*. Birds have primate-like numbers of neurons in the forebrain. *Proc Natl Acad Sci USA*. 2016;**113**:7255–7260.
34. Atoji Y, *et al*. Differential projections of the densocellular and intermediate parts of the hyperpallium in the pigeon (Columba livia). *J Comp Neurol*. 2018;**526**(1):146–165.
35. Karten HJ, *et al*. Neural connections of the "visual wulst" of the avian telencephalon. Experimental studies in the pigeon (Columba livia) and owl (Speotyto cunicularia). *J Comp Neurol*. 1973;**150**:253–277.
36. Watanabe M, *et al*. Cytoarchitecture and visual receptive neurons in the Wulst of the Japanese quail (Coturnix coturnix japonica). *J Comp Neurol*. 1983;**213**(2):188–198.
37. Wild JM. Thalamic projections to the paleostriatum and neostriatum in the pigeon (Columba livia). *Neuroscience*. 1987;**20**(1):305–327.
38. Ng BS, *et al*. Dominant vertical orientation processing without clustered maps: early visual brain dynamics imaged with voltage-sensitive dye in the pigeon visual Wulst. *J Neurosci*. 2010;**30**(19):6713–6725.
39. Karten HJ, *et al*. *A Stereotaxic Atlas of the Brain of the Pigeon (Columba Livia)* Baltimore, MD: Johns Hopkins Press; 1967.
40. Reiner A, *et al*. The laminar source of efferent projections from the avian Wulst. *Brain Res*. 1983;**275**(2):349–354.

41. Shanahan M, *et al*. Large-scale network organization in the avian forebrain: a connectivity matrix and theoretical analysis. *Front Comput Neurosci*. 2013;**7**:89.
42. Rattenborg NC, *et al*. Hippocampal memory consolidation during sleep: a comparison of mammals and birds. *Biol Rev Camb Philos Soc*. 2011;**86**(3):658–691.
43. Engelage J, *et al*. The organization of the tectofugal pathway in birds: a comparative review. In: Zeigler H, ed. *Vision, Brain, and Behavior in Birds*. Cambridge, Mass: MIT Press; 1993: 137–158.
44. Martinez-Gonzalez D, *et al*. Increased EEG spectral power density during sleep following short-term sleep deprivation in pigeons (Columba livia): evidence for avian sleep homeostasis. *J Sleep Res*. 2008;**17**(2):140–153.
45. Luan L, *et al*. Ultraflexible nanoelectronic probes form reliable, glial scar-free neural integration. *Sci Adv*. 2017;**3**:e1601966.
46. van der Walt S, *et al*. The NumPy array: a structure for efficient numerical computation. *Comput Sci Eng*. 2011;**13**:22–30.
47. Jones E, *et al*. SciPy: Open Source Scientific Tools for Python. 2001–2018 https://www.scipy.org/scipylib/download.html
48. Beckers GJ, *et al*. Plumes of neuronal activity propagate in three dimensions through the nuclear avian brain. *BMC Biol*. 2014;**12**:16.
49. Voirin B, *et al*. Ecology and neurophysiology of sleep in two Wild Sloth species. *Sleep*. 2014;**37**:753–761.
50. Ayala-Guerrero F, *et al*. Sleep characteristics in the turkey Meleagris gallopavo. *Physiol Behav*. 2003;**78**(3):435–440.
51. Low PS, *et al*. Mammalian-like features of sleep structure in zebra finches. *Proc Natl Acad Sci USA*. 2008;**105**:9081–9086.
52. Fiáth R, *et al*. Large-scale recording of thalamocortical circuits: in vivo electrophysiology with the two-dimensional electronic depth control silicon probe. *J Neurophysiol*. 2016;**116**(5):2312–2330.
53. Fiáth R, *et al*. Laminar analysis of the slow wave activity in the somatosensory cortex of anesthetized rats. *Eur J Neurosci*. 2016;**44**(3):1935–1951.
54. Borbély AA, *et al*. A single dose of benzodiazepine hypnotics alters the sleep EEG in the subsequent drug-free night. *Eur J Pharmacol*. 1983;**89**(1–2):157–161.
55. Lancel M, *et al*. Pregnenolone enhances EEG delta activity during non-rapid eye movement sleep in the rat, in contrast to midazolam. *Brain Res*. 1994;**646**(1):85–94.
56. Lancel M, *et al*. Role of GABAA receptors in sleep regulation. Differential effects of muscimol and midazolam on sleep in rats. *Neuropsychopharmacology*. 1996;**15**(1):63–74.
57. Tobler I, *et al*. Diazepam-induced changes in sleep: role of the alpha 1 GABA(A) receptor subtype. *Proc Natl Acad Sci USA*. 2001;**98**(11):6464–6469.
58. Kopp C, *et al*. Diazepam-induced changes on sleep and the EEG spectrum in mice: role of the alpha3-GABA(A) receptor subtype. *Eur J Neurosci*. 2003;**17**(10):2226–2230.
59. Kopp C, *et al*. Modulation of rhythmic brain activity by diazepam: GABA(A) receptor subtype and state specificity. *Proc Natl Acad Sci USA*. 2004;**101**(10):3674–3679.
60. Timofeev I, *et al*. Disfacilitation and active inhibition in the neocortex during the natural sleep-wake cycle: an intracellular study. *Proc Natl Acad Sci USA*. 2001;**98**:1924–1929.
61. Szymczak JT, *et al*. A study of sleep in the European blackbird. *Physiol Behav*. 1996;**60**(4):1115–1120.
62. Jones SG, *et al*. Homeostatic regulation of sleep in the white-crowned sparrow (Zonotrichia leucophrys gambelii). *BMC Neurosci*. 2008;**9**:47.
63. Scriba MF, *et al*. Linking melanism to brain development: expression of a melanism-related gene in barn owl feather follicles covaries with sleep ontogeny. *Front Zool*. 2013;**10**(1):42.
64. Franken P, *et al*. High-frequency components of the rat electrocorticogram are modulated by the vigilance states. *Neurosci Lett*. 1994;**167**(1–2):89–92.
65. Maloney KJ, *et al*. High-frequency gamma electroencephalogram activity in association with sleep-wake states and spontaneous behaviors in the rat. *Neuroscience*. 1997;**76**(2):541–555.
66. Brankack J, *et al*. EEG gamma frequency and sleep-wake scoring in mice: comparing two types of supervised classifiers. *Brain Res*. 2010;**1322**:59–71.
67. Llinás R, *et al*. Coherent 40-Hz oscillation characterizes dream state in humans. *Proc Natl Acad Sci USA*. 1993;**90**:2078–2081.
68. Mann K, *et al*. Dynamical properties of the sleep EEG in different frequency bands. *Int J Neurosci*. 1993;**73**(3–4):161–169.
69. Rubino D, *et al*. Propagating waves mediate information transfer in the motor cortex. *Nat Neurosci*. 2006;**9**(12):1549–1557.
70. Dudai Y, *et al*. The consolidation and transformation of memory. *Neuron*. 2015;**88**(1):20–32.
71. Ditz HM, *et al*. Neurons in the hippocampus of crows lack responses to non-spatial abstract categories. *Front Syst Neurosci*. 2018;**12**:33.
72. Gais S, *et al*. Learning-dependent increases in sleep spindle density. *J Neurosci*. 2002;**22**(15):6830–6834.
73. Tamminen J, *et al*. The role of sleep spindles and slow-wave activity in integrating new information in semantic memory. *J Neurosci*. 2013;**33**(39):15376–15381.
74. Huber R, *et al*. Local sleep and learning. *Nature*. 2004;**430**(6995):78–81.
75. Rattenborg NC, *et al*. Sleep locally, act globally. *Neuroscientist*. 2012;**18**(5):533–546.
76. Vyazovskiy VV, *et al*. Sleep and the single neuron: the role of global slow oscillations in individual cell rest. *Nat Rev Neurosci*. 2013;**14**(6):443–451.
77. Contreras D, *et al*. Spatiotemporal patterns of spindle oscillations in cortex and thalamus. *J Neurosci*. 1997;**17**(3):1179–1196.
78. Contreras D, *et al*. Spindle oscillations during cortical spreading depression in naturally sleeping cats. *Neuroscience*. 1997;**77**(4):933–936.
79. Destexhe A, *et al*. Spatiotemporal analysis of local field potentials and unit discharges in cat cerebral cortex during natural wake and sleep states. *J Neurosci*. 1999;**19**(11):4595–4608.
80. Miceli D, *et al*. Extratelencephalic projections of the avian visual Wulst. A quantitative autoradiographic study in the pigeon Columbia livia. *J Hirnforsch*. 1987;**28**(1):45–57.
81. Watanabe M. Synaptic organization of the nucleus dorsolateralis anterior thalami in the Japanese quail (Coturnix coturnix japonica). *Brain Res*. 1987;**401**(2): 279–291.
82. Wild JM, *et al*. Rostral wulst in passerine birds. I. Origin, course, and terminations of an avian pyramidal tract. *J Comp Neurol*. 2000;**416**(4):429–450.
83. Miceli D, *et al*. Fine structure of the visual dorsolateral anterior thalamic nucleus of the pigeon (Columba livia): a hodological and GABA-immunocytochemical study. *J Comp Neurol*. 2008;**507**(3):1351–1378.
84. Vorster AP, *et al*. Sleep and memory in mammals, birds and invertebrates. *Neurosci Biobehav Rev*. 2015;**50**:103–119.